An optical fibre dynamic instrumented palpation sensor for the characterisation of biological tissue

Li, J.; Hammer, Steven J; Shu, Wenmiao; Maier, Robert Raimund; Hand, Duncan Paul; Reuben, Robert Lewis; MacPherson, William Neil

Published in:
Sensors and Actuators A: Physical

DOI:
10.1016/j.sna.2015.01.036

Publication date:
2015

Sensors and Actuators A 225 (2015) 53–60

Contents lists available at ScienceDirect

Sensors and Actuators A: Physical

journal homepage: www.elsevier.com/locate/sna

An optical fibre dynamic instrumented palpation sensor for the characterisation of biological tissue

J. Li[a,b,1], S.J. Hammer[c,*,1], W.M. Shu[d], R.R.J. Maier[a], D.P. Hand[a], R.L. Reuben[c], W.N. MacPherson[a]

[a] Institute of Photonics and Quantum Sciences, SUPA, Heriot-Watt University, Edinburgh EH14 4AS, UK
[b] Anhui Provincial Key Laboratory of Photonic Devices and Materials, Anhui Institute of Optics and Fine Mechanics, Chinese Academy of Sciences, Hefei 230031, China
[c] Institute of Mechanical, Process and Energy Engineering, Heriot-Watt University, Edinburgh EH14 4AS, UK
[d] Institute of Biological Chemistry, Biophysics and Bioengineering, Heriot-Watt University, Edinburgh EH14 4AS, UK

ARTICLE INFO

Article history:
Received 29 May 2014
Received in revised form
11 December 2014
Accepted 30 January 2015
Available online 9 February 2015

Keywords:
Membrane
Interferometer
Soft tissue
Palpation
Fabry–Pérot

ABSTRACT

The diagnosis of prostate cancer using invasive techniques (such as biopsy and blood tests for prostate-specific antigen) and non-invasive techniques (such as digital rectal examination and trans-rectal ultrasonography) may be enhanced by using an additional dynamic instrumented palpation approach to prostate tissue classification. A dynamically actuated membrane sensor/actuator has been developed that incorporates an optical fibre Fabry–Pérot interferometer to record the displacement of the membrane when it is pressed on to different tissue samples. The membrane sensor was tested on a silicon elastomer prostate model with enlarged and stiffer material on one side to simulate early stage prostate cancer. The interferometer measurement was found to have high dynamic range and accuracy, with a minimum displacement resolution of ±0.4 μm over a 721 μm measurement range. The dynamic response of the membrane sensor when applied to different tissue types changed depending on the stiffness of the tissue being measured. This demonstrates the feasibility of an optically tracked dynamic palpation technique for classifying tissue type based on the dynamic response of the sensor/actuator.

1. Introduction

Prostate cancer is the most commonly diagnosed cancer in men [1]. In common with other cancers, early diagnosis improves the possible outcome for the patient. At present diagnosis of prostate cancer is carried out using four main methods: digital rectal examination (DRE); a prostate-specific antigen (PSA) blood test; prostate biopsy, and trans-rectal ultrasound (TRUS), often incorporating trans-rectal sonoelastography (TRSE).

DRE is a straightforward but subjective test, where the prostate is palpated using the fingertip. Palpation reveals if the prostate is enlarged, and may also reveal the presence of hard nodules which are indicative of cancer [2]. DRE is highly subjective and depends strongly on the skill and experience of the medic performing the examination [3]. In addition, DRE may only have higher levels of accuracy when prostate cancer is at a more advanced stage, which limits its utility as a tool for early stage disease detection. Alternatively a blood test designed to identify high levels of prostate-specific antigen (PSA) for prostate cancer diagnosis may offer earlier detection. Unfortunately the use of the PSA test has been subject to a high rate of false-positive results, leading to unnecessary surgery [2]. In addition, some types of cancer may not cause the production of PSA, which further reduces the reliability of the test. A positive result based upon palpation or PSA tests often results in a prostate biopsy. In this procedure needles are inserted into the prostate and core samples of the gland are removed for histological analysis. The samples are assessed using the Gleason Grade for tissue quality [4] and following these tests, a patient may be recommended for surgery. TRUS and TRSE [5] are also used to diagnose the extent of prostate cancer. In a TRUS examination, the ultrasound transducer is inserted into the rectum and images the prostate *via* its posterior surface. Some types of tumour are visible as anechoic regions in the ultrasound image. TRSE adds a coloured overlay showing tissue stiffness to the image captured using TRUS. In most TRSE probes, an inflatable cuff is attached to the protective sheath over the probe. The cuff is inflated and deflated, usually by hand, to compress and release the tissue around the probe. The

* Corresponding author. Tel.: +44 131 451 3614; fax: +44 1314513129.
E-mail address: s.hammer@hw.ac.uk (S.J. Hammer).
[1] Joint first authors.

http://dx.doi.org/10.1016/j.sna.2015.01.036

changes in the image between compression cycles are processed to produce a colour map of (usually relative) stiffness of the tissue in the prostate.

A primary problem with these four common diagnostic methods is low sensitivity and specificity. DRE is unlikely to be able to distinguish small nodules of potentially malignant cancer. A biopsy may miss the cancerous regions of the gland altogether, resulting in a misleading assessment of the type and extent of cancer present. Failures in these diagnostic tools mean that some men undergo unnecessary prostate surgery.

Inadequacies in the current diagnostic tools for prostate cancer diagnosis have led to the development of a dynamic instrumented palpation (DIP) [6] device to measure prostate stiffness and diagnose disease type based on the mechanical properties of the tissue. A DIP device palpates the prostate gland at a controlled frequency and allows the dynamic and static behaviour of the tissue to be measured. This allows measurement of the shear modulus and Young's modulus of the prostate gland, both of which can be used to identify stiffer regions indicative of prostate cancer [7].

A DIP device made in this way can be inserted rectally and a pressure deformable membrane used to palpate the posterior surface of the prostate gland in a similar manner to current DRE practice. The advantage of the device over DRE is that a *quantitative* measurement of stiffness is given that can be compared to other measurements of prostate stiffness and used to diagnose more accurately the presence of prostate cancer.

There have been other attempts at creating a resonant sensor system for measuring the stiffness of the prostate gland. Most other groups have used a resonant actuator that is mounted above an *ex vivo* tissue sample [8–10]. These usually consist of a controlled motion stage linked to a load cell measuring the load applied to the sample. A primary disadvantage of most resonant sensor systems is that the sensor actuator and sensing system are too large to be used *in vivo*.

However a challenge remains in miniaturising the instrumentation used for monitoring the deflection of the deformable membrane. An electrical strain gauge (for example) bonded to the sensor membrane could measure strain as a function of motion but would increase its inertia, which may reduce its sensitivity to small motions. In addition, the strain gauge dimensions limit sensor miniaturisation. An alternative approach is to use optical techniques to monitor the membrane deflection. An optical fibre-based approach is highly miniaturisable, since the size of the measurement point is dictated by the sub-millimetre diameter of the fibre. The non-contact nature of the measurement also means that the measurement system does not influence the motion of the dynamic sensor. This allows the creation of smaller scale sensors that may be used to measure the micro-mechanical properties of tissue.

Therefore, in this paper, we designed and manufactured a prototype fibre optic membrane sensor (the "p-finger") based on a Fabry–Pérot interferometer. A DIP device was developed with a flexible membrane that is inflated and deflated at a controlled frequency. The device was tested on a model prostate gland with a unilateral enlarged region simulating early stage prostate cancer. The relative stiffness of the two sides of the model prostate gland was evaluated by comparing the change in dynamic response of the membrane when it is pressed on sites with and without the simulated cancerous region.

2. Sensing principle

The p-finger consists of a dynamically actuated flexible membrane. The displacement of the membrane is measured using a fibre optic interferometer mounted beneath the membrane to create a Fabry–Pérot interferometer [11]. The p-finger is pressed on to a tissue sample and the change in the dynamic displacement response of the membrane is measured. The change in membrane response is related to the mechanical properties of the tissue being measured. In principle, this allows regions of different tissue types to be distinguished based on the change in measured membrane behaviour.

Fabry–Pérot interferometer-based sensor systems have had previous medical sensor applications. In [12] this type of sensor was used to give force feedback during vitreoretinal microsurgery. A Fabry–Pérot device with a MEMS membrane pressure sensor has also been used to monitor blood flow pressure in the heart [13]. An additional application includes sensing the pressure changes in the pharynx during swallowing [14].

There are various other optical fibre-based sensors which can be used to detect displacement and strain. Fibre-Bragg grating sensors are extensively used but potentially too large for this application [15]. Intensity-based optical fibre sensors can have repeatability problems due to connector losses [16] which do not affect the sensor reported here. Other membrane-based optical sensors have also been developed for non-medical applications. These include a micromachined silicon diaphragm sensor used for pressure measurement [17] and a peninsula-structured diaphragm with a piezoresistive pressure sensor [18].

The deflection of the p-finger membrane can be accurately monitored using interferometry. Light is reflected from the membrane

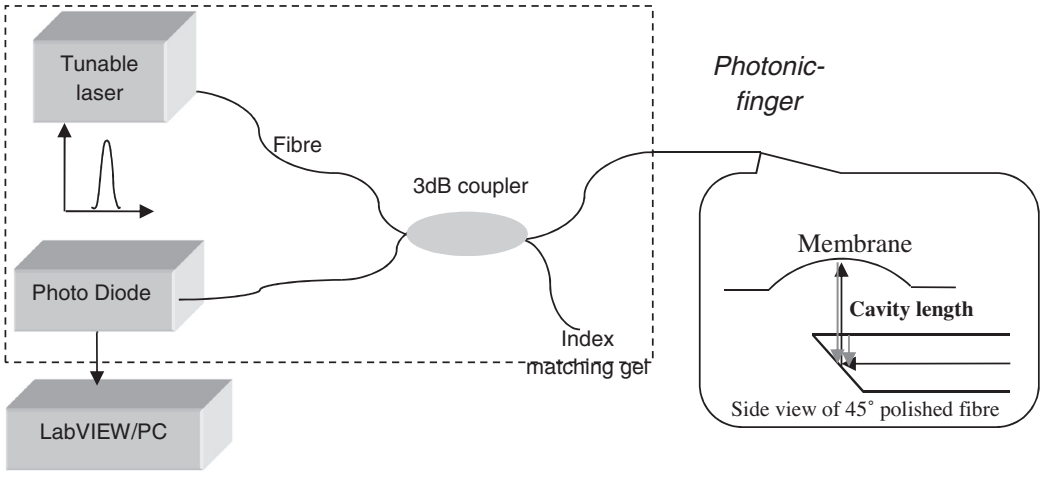

Fig. 1. Left: a schematic of the optical interrogation system, where the tuneable source is incident on the sensor *via* a 3 dB 2 × 2 coupler. The coupler allows the reflected signal to be directed onto a photodetector. Right: the details of the cavity formed between the membrane and a 45° polished fibre.

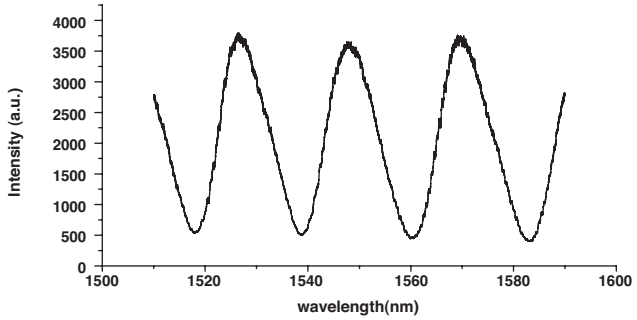

Fig. 2. A typical reflection interferogram measured across the p-finger membrane cavity.

and mixed with light reflected from a stable reference surface, with the resulting signal depending upon the membrane position. To miniaturise the sensor we require a configuration where the membrane is aligned parallel with the optical fibre. Therefore we require a 45° mirror that is mechanically polished onto the fibre to allow light from the fibre to be reflected to the membrane, as shown in Fig. 1. The interferometer is formed between the membrane and fibre sidewall. The reflected signals are coupled back into the optical fibre using the 45° polished fibre mirror for detection at a remote location. The mirror surface is metal coated to enhance its reflectivity.

When the membrane is pressed on to the model prostate gland, it is deflected. This in turn changes the cavity length between the membrane and the fibre. A typical reflection interferogram is shown in Fig. 2, where the fringe spacing (termed the free spectral range [19]) is related to the cavity length. The measured cavity length can be calculated by using the FFT algorithm to determine the fringe spacing [20]. From this a measure of cavity length with 0.4 μm resolution over a 721 μm range is demonstrated.

The static cavity length fluctuation over 1 h 25 min is shown in Fig. 3, where the calculated RMS error of cavity fluctuation is less than ±0.4 μm. For the device, the absolute cavity length is 721 μm calculated using an FFT algorithm. This will be the reference measurement point of the sensor to measure the dynamic behaviour of the membrane. This means the relative RMS error is ±0.53%. This error is larger than that achieved elsewhere (for example in [19]), since here the front part of the 45° polished fibre is a cantilevered component held in place using epoxy adhesive. Small vibrations of the fibre will lead to the deflection of the tip and cause a measured

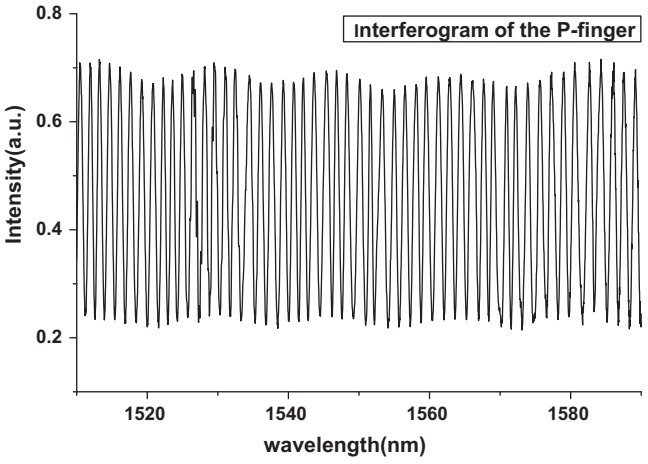

Fig. 3. A typical interferogram from the p-finger sensor. In this case the cavity length is 721 μm.

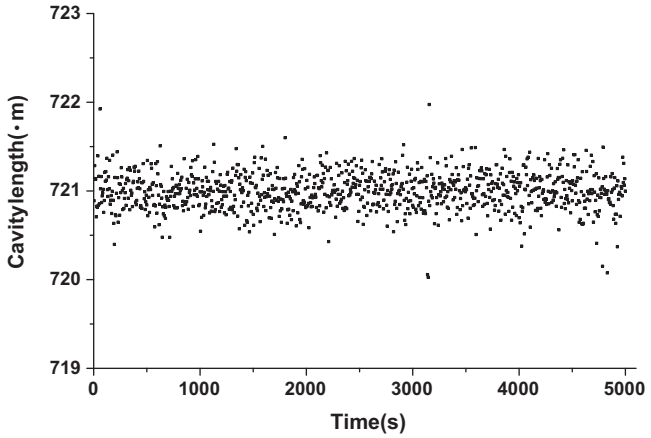

Fig. 4. Cavity length fluctuation over time of the membrane sensor.

cavity length change. In addition, any thermal gradients will affect the deformation of the cantilevered fibre end, which will also add to the cavity length fluctuation. However, the measurement error here is already much smaller than that expected with an electrical resistance strain gauge. This demonstrates that the sensor is capable of measuring a large dynamic range while maintaining a high spatial resolution.

The achievable spatial resolution of the sensor is dependent on the size of the sensing location given by the optical fibre, and the stiffness of the membrane material used. The optical fibre has a measurement spot size of 125 μm diameter. This implies that the main limitation on scaling down the sensor spatial resolution is the membrane material. The current sensor membrane diameter of 10 mm was chosen to resemble the sensing area of a human fingertip. With this technology, a scalable family of sensors could be created with spatial resolution limited only by the membrane size that will support a measurable inflation sufficient to reach above the outer rim area of the top layer of the device and palpate tissue.

3. Sensor fabrication

The fabrication of the sensor can be divided into two steps: forming the body of the sensor from laser cut acrylic layers, and inserting and aligning the optical fibre sensor.

The body of the sensor was fabricated from several layers of laser-cut and engraved acrylic which were held together with contact adhesive (Fig. 4). The device is 27 mm long by 14 mm wide by 5 mm deep. The main layer of the device was formed from 3 mm thick acrylic sheet. The membrane was held in place by adhesive attached to the cap and the air channel layer, and inflates through the 10 mm diameter hole in the cap. Cut-outs for bayonet tube connections were formed in the main layer. The tube connections were fixed in place using epoxy cement. The air channel layer also has a support channel sized to fit the cladding of the bare optical fibre. The layer above this has a bridge piece with a hole which is aligned with the centre of the membrane. The bridge supports the optical fibre and provides a guide for its insertion and alignment with the membrane centre. Silicon tubing was fitted on to the barbed tube connections and then used to attach to 1.6 mm outer diameter PTFE tubing. The tubing was attached to a syringe which was manually actuated to inflate and deflate the membrane. The system was leak checked before measurement to avoid spurious motion of the membrane due to leakage.

An SMF-28 optical fibre was mechanically polished to 45° (Fig. 5) and then inserted into the channel in the bridge. By carefully

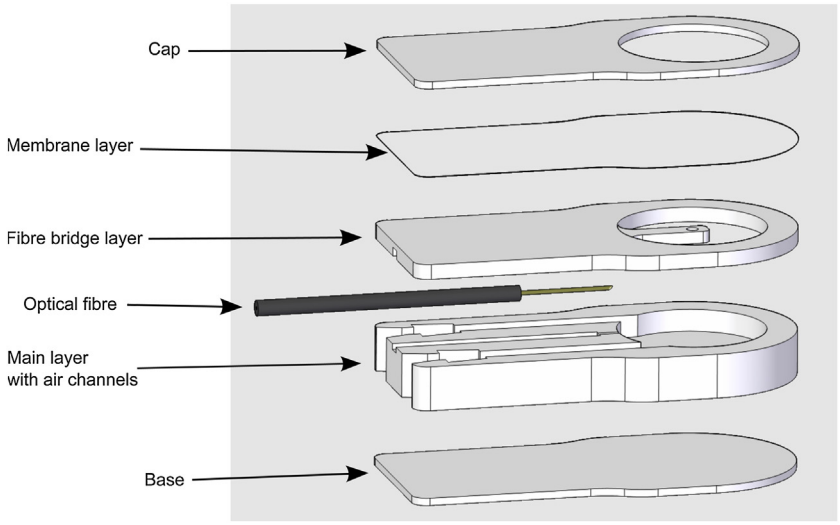

Fig. 5. An exploded view of the sensor. The air supply tubing and fittings incorporated into the main layer have been omitted for clarity.

aligning the position of the fibre while monitoring the interferogram, a Fabry–Pérot (FP) interferometer can be formed between the fibre tip and membrane [20]. To aid positioning of the fibre, the partially assembled device and the fibre were mounted onto a three dimensional translation stage. The polished fibre was held on a rotation stage which was able to rotate through 360° with a 5° resolution. The fibre is carefully inserted into the sensor housing by gently pushing the translation stage. Then the fibre is rotated slightly until clearly visible fringes between the fibre and diaphragm can be seen using the interrogation system described in [20]. The fully assembled device is shown in Fig. 6. The membrane was a 50 μm thick silicone-based film. The centreline of the optical fibre was placed approximately 0.9 mm below the lower surface of the membrane when at rest (and measured to be 0.72 mm using a SM125 interrogator (Micron Optics, USA) based on the interferometric principle). The distance between the lower surface of the membrane and the tip of the polished fibre is normally controlled to be ~1 μm to receive sufficient reflected light for measurement. The entire sensor was hand-assembled with the aid of the positioning stages described above. For mass manufacture of the sensor, accurate control of the distance between the end of the fibre and the lower surface of the membrane would be required.

4. Results and discussion

4.1. Sensor calibration

Calibration aims to test the static performance of the p-finger as the membrane is actuated by varying the pressure behind the membrane. In this way, air leakage can be identified and the deflection of the membrane can be calibrated against pressure change.

For a clamped circular membrane undergoing small deflections (defined as less than half of the thickness of the membrane), the peak deflection can be expressed as

$$y_p = \frac{3(1-\mu^2)a^4}{8nEh^3} \quad (1)$$

where y_p is the deflection at the central point; μ is Poisson's ratio; E is the Young's modulus of the membrane material; n is the refractive index of the medium (in this case, air); a is the radius of the membrane and h is the thickness of the membrane [21].

The calibration experiment is set-up as shown in Fig. 7, where a manometer is used for pressure calibration. One end of the manometer is open to air while the other end is connected with tubing to the outlet of the sensor. The inlet of the sensor is connected to a syringe by a plastic tube. An SM-125 optical interrogator (Micron

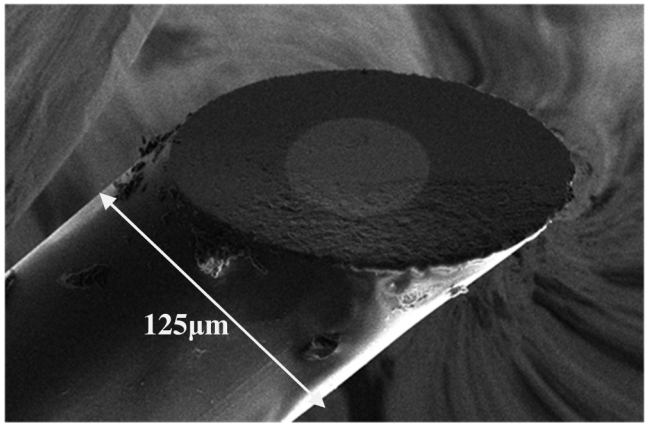

Fig. 6. An SEM of the end of the optical fibre showing the 45° polished surface. The circular central area is metal coated to improve the reflectivity. The surface roughness is measured to be in the region of tens of nm, which is suitable for this application.

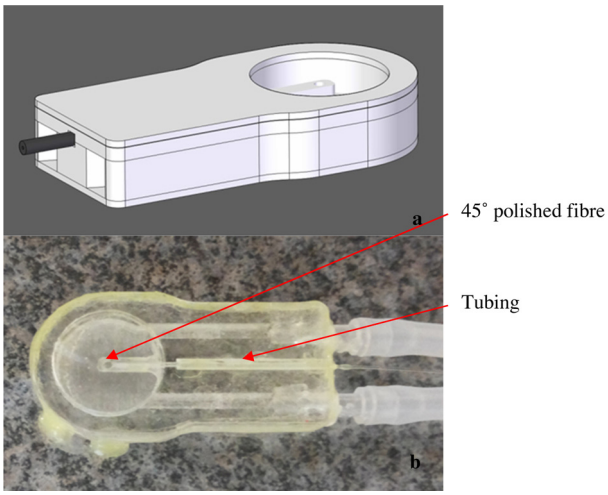

Fig. 7. Top: a CAD rendering of the fully assembled device. Bottom: the completed device. The overall length of the device is 25 mm.

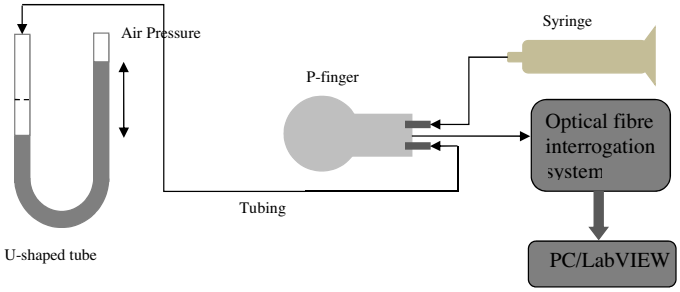

Fig. 8. A schematic diagram of the manometer (U-tube) apparatus used to calibrate the pressure/displacement response of the p-finger membrane.

Optics Inc., GA, USA) is used to acquire the interference fringes from the sensor and a custom LabVIEW program is used to demodulate the cavity length. The pressure inside the membrane, varied by the syringe, will make the membrane deflect. This displacement can then be measured and converted to the pressure applied to the membrane. The difference in water height in the manometer is proportional to the pressure difference. By measuring the difference in height, the pressure difference can be calculated. The demodulated peak deflection of the membrane was plotted against the pressure difference between the atmosphere pressure and the syringe pumping pressure (Fig. 8). At each pressure, five deflection measurements were taken. Pressures between 200 and 900 Pa were monitored. Both a forward cycle with increasing pressure and a backward cycle with decreasing pressure were tested. Another two more sets of measurements with both forward and backward cycling were acquired showing a similar pressure trend. The pressure cycling response of the membrane can be fitted with a linear fit as shown in Fig. 8.

It can be seen that a large deflection range of up to 1000 μm with a nearly linear response is achieved under slowly varying pressure excitation. Both the forward and backward cycling show that the sensor can operate in a large deflection range while maintaining a linear response and without significant signs of any hysteresis.

4.2. Dynamic measurement of membrane deflection

The aim of dynamic measurement is to test the mechanical response from the simulated prostate tissue by applying a compressive dynamic strain to the sample. This is achieved by modulating the peak deflection of the membrane with a sinusoidal excitation and measuring its response. In the case of dynamic measurement, the sensor operates at a fixed cavity length and a small fraction of deflection excited by the pumping pressure will be detected. A schematic diagram of the dynamic measurement apparatus is shown in Fig. 9. A tuneable laser-based interrogation system [21] is employed for dynamic measurement, operating near the quadrature point of the interferogram [22] to achieve a near linear response with respect to the applied signal. The membrane was illuminated using a 1532 nm wavelength laser diode. The reflected light from the test sample was then recorded by a photo-diode and converted to an electronic signal. In this case, since the change in pressure is very small, the measured membrane deflection will also be very small. The relation between the deflection change and the interfered fringe change in the spectrum domain can be expressed by

$$\frac{\Delta\lambda}{\lambda} = \frac{\Delta d}{d} \quad (2)$$

where λ is the laser operation wavelength, d is the absolute cavity length (which here refers to the distance between the polished fibre and the membrane), Δd is the pressure induced deflection change, and $\Delta\lambda$ is the deflection induced fringe shift. In our case, s is 1532 nm, d is ~731 s and Δn is normally <1 μm. The deflection induced fringe shift is within the linear range if the laser operates near the quadrature point [23].

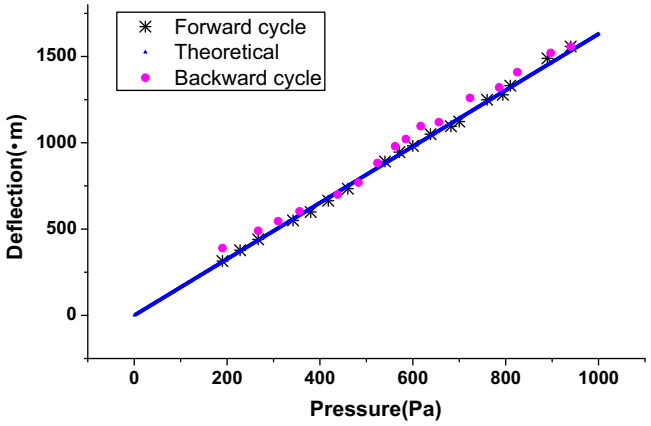

Fig. 9. The deflection response of the membrane due to changing pressure applied to the sensor. The deflection error for a fixed pressure is within 200 nm at each point, which is too small to be visible on the deflection scale.

The model prostate gland is mounted on a three axis linear stage. The membrane sensor is mounted on top of the stage and pressed down to contact the sample. Before measurement begins, the zero pressure position for the membrane must be calibrated. This is achieved by gently pushing the device so the membrane just contacts the surface of the model prostate gland, and then carefully adjusting the vertical position of the sensor until the output signal from the interrogation system is stable. This ensures that the cavity length between the centre of the membrane and the fibre has not changed and there was no additional pressure applied on the sample.

The pressure inside the membrane chamber is dynamically actuated with a sinusoidal pressure wave using a syringe pump. 5 Hz, 15 Hz and 20 Hz sinusoidal signals were used to actuate the syringe pump, thus modulating the deflection of the membrane. Previous work has suggested that actuation frequencies in this range produce a large response from prostate tissue [24]. The reflected deflection after the membrane contacts the model prostate gland is monitored using the single wavelength laser interrogation system.

Changes in the amplitude and phase relationship of the applied air pressure and measured membrane deflection signals are related to the stiffness of the material being measured. The amplitude of the deflection signal is reduced as the membrane touches the prostate model. The size of the reduction in deflection is related to the stiffness of the material being touched. In addition, when the prostate model is touched by the membrane, a phase shift occurs between the applied air pressure and the displacement of the membrane. The phase shift is related to the shear modulus of the material [7].

4.3. Measured displacements when touching the diseased and healthy sides of the prostate model

A typical response of the excited sine signal before and after touching the simulated prostate cancer tissue is shown in Fig. 10. The response before and after touching the simulated healthy tissue is shown in Fig. 11.

The contact distance between the sensor diaphragm and the tissue is controlled by monitoring the intensity variation from the interrogation system. This point should be carefully controlled so that the there is no DC change from the interrogation system after the diaphragm begins to contact the model surface. On touching the diseased side of the model prostate gland (Fig. 10), a

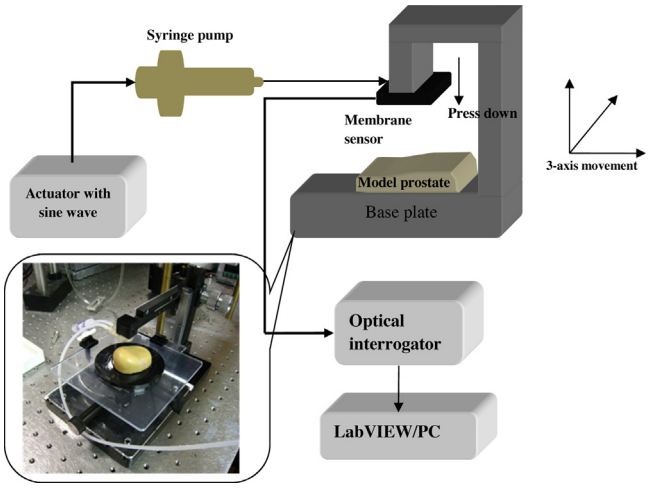

Fig. 10. Experimental set-up for dynamic testing of the model prostate.

larger reduction in the amplitude of the measured displacement is observed than when touching the healthy side (Fig. 11). The larger reduction is due to the increased stiffness of the diseased region of the model, which increases the stiffness of the membrane and diseased tissue combination, thus reducing the ability of the air supply to inflate the membrane to its unloaded peak displacement.

4.4. Distinguishing tissue type based on amplitude and phase change

The dynamic behaviour of different materials may be distinguished using two parameters. The first parameter, amplitude ratio (AR), is defined as

$$\mathrm{AR} = \frac{\text{amplitude (membrane deflection in air)}}{\text{amplitude (membrane delfection in contact with tissue)}} \quad (3)$$

where membrane displacements are measured in μm. This is related to the elastic behaviour of the material being measured. The second parameter is the tangent of the phase difference between the displacement waveform before and after contacting the tissue. This is expressed as tan(θ), which is related to the shear modulus of the material.

The AR and phase difference were calculated from a 5 s long portion of the loaded signals. For each measurement, the p-finger was held in place on the prostate model and actuated.

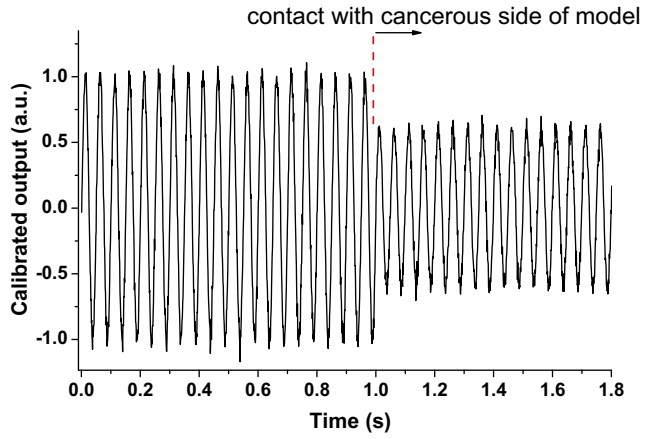

Fig. 11. The change in the dynamic deflection of the membrane before and after touching the side of the model prostate gland with prostate cancer.

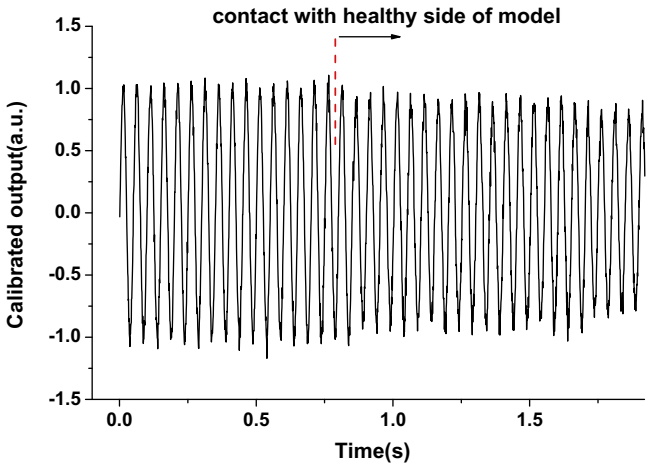

Fig. 12. The change in the dynamic deflection of the membrane before and after touching the healthy side of the model prostate gland.

4.5. Healthy and prostate cancer model tissue behaviour at different actuation frequencies

The dynamic behaviour of real biological materials can vary with the frequency of the applied loading. To test the ability of the p-finger to distinguish prostate cancer from healthy tissue at different frequencies, it was used to dynamically load the model at 5, 15 and 20 Hz. Three positions on each side of the model were chosen, and measurements of membrane displacement at each frequency were made at each position. To distinguish between prostate cancer and healthy tissue, AR was plotted against tan(θ) (Fig. 12). Two regions of data emerge, showing a cluster of prostate cancer measurements with low phase difference and high AR, and a cluster of healthy tissue measurements showing high phase difference and low AR. AR in this case is a measure of the dynamic stiffness response of the material. In stiffer (more diseased) tissue, it is expected that AR will increase since the membrane/tissue coupling will respond less to the dynamic loading from the air supply. It has previously been reported [25] that cancerous tissue exhibits a smaller phase difference between the actuation and sensor signals in a resonant mechanical sensor system. Healthy prostate tissue has larger fluid-filled glandular structures. These have a higher proportion of viscoelastic material which increases the damping of the

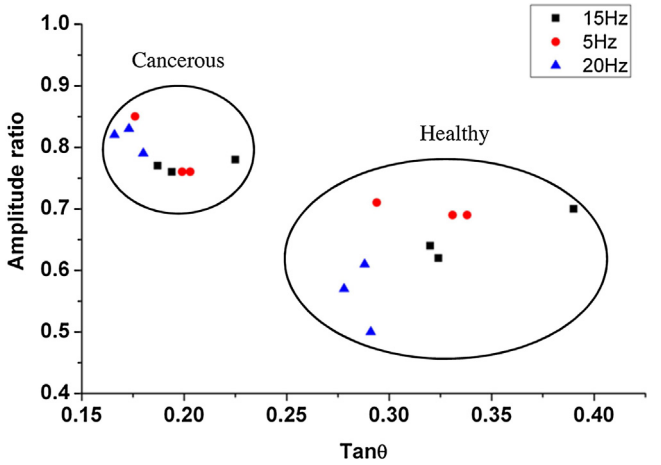

Fig. 13. Prostate cancer may be distinguished from healthy tissue in the prostate model at different actuation frequencies. The plot of amplitude ratio against the tangent of the phase difference between the excitation signal and the measured displacement shows distinct clusters of prostate cancer and healthy results.

material. This slows the response of the sensor, and causes a relative increase in the phase difference. In contrast, cancerous tissue has smaller fluid-filled structures, which reduce the damping effect on the sensor (Fig. 13).

One limitation of this study is the realism of the prostate model used. The model is made from silicone elastomer moulded into an approximation of the shape of a real prostate. One side of the model is more enlarged and stiffer than the other side. This is intended to model the geometry change inherent in benign prostate hyperplasia and early stage prostate cancer. The material composition of a real prostate with prostate cancer is more complex than this model. However, the model is designed primarily as a training aid with a long shelf life, meaning that stable materials suitable for long-term use were used in its construction. An improved prostate model with embedded tumours at a known depth and with known mechanical properties would give a fuller assessment of the utility of the p-finger in sensing and characterising tissue type.

5. Conclusion

We have developed an optical dynamic instrumented palpation sensor for the measurement of tissue stiffness. The sensor, named the p-finger, consists of a dynamically actuated membrane with a polished optical fibre underneath. A Fabry–Pérot interferometer is formed between the end of the fibre and the inner surface of the membrane, which gave a displacement accuracy of ±0.4 μm over a deflection range of 721 μm. We used the sensor to measure the stiffness of a model prostate gland with unilateral early stage cancer, and were able to distinguish simulated prostate cancer tissue from healthy tissue. The relationship between the amplitude and the phase of the displacement and actuation waveforms were used to distinguish each tissue type. Further work will include studies on excised human prostate tissue to develop methods of reliably diagnosing prostate cancer.

Acknowledgements

Jun Li received a studentship from the Scottish Universities Physics Alliance and was also funded by the James Watt Institute for High Value Manufacturing (under the UK Engineering and Physical Sciences Research Council (EPSRC) grant no. EP/F02553X/1. S.J. Hammer was funded by the EPSRC under grant no. EP/I019472/1.

References

[1] A. Jemal, F. Bray, M.M. Center, J. Ferlay, E. Ward, D. Forman, Global cancer statistics, CA Cancer J. Clin. 61 (March (2)) (2011) 69–90.
[2] S.R. Gambert, Screening for prostate cancer, Int. Urol. Nephrol. 33 (June (2)) (2001) 249–257.
[3] L.A. Baumgart, G.J. Gerling, E.J. Bass, Characterizing the range of simulated prostate abnormalities palpable by digital rectal examination, Cancer Epidemiol. 34 (February (1)) (2010) 79–84.
[4] D.F. Gleason, Histologic grading of prostate cancer: a perspective, Hum. Pathol. 23 (March (3)) (1992) 273–279.
[5] L. Pallwein, M. Mitterberger, G. Pinggera, F. Aigner, F. Pedross, J. Gradl, A. Pelzer, G. Bartsch, F. Frauscher, Sonoelastography of the prostate: comparison with systematic biopsy findings in 492 patients, Eur. J. Radiol. 65 (February (2)) (2008) 304–310.
[6] S.A. McNeill, R.L. Reuben, Apparatus for mapping biological tissue quality, US2006051734 (A1) (9 March 2006).
[7] Y.-C. Fung, Biomechanics: Mechanical Properties of Living Tissues, Springer, 1993.
[8] B. Ahn, E.I.S. Lorenzo, K.H. Rha, H.J. Kim, J. Kim, Robotic palpation-based mechanical property mapping for diagnosis of prostate cancer, J. Endourol. 25 (April (5)) (2011) 851–857.
[9] V. Jalkanen, B.M. Andersson, A. Bergh, B. Ljungberg, O.A. Lindahl, Indentation loading response of a resonance sensor – discriminating prostate cancer and normal tissue, J. Med. Eng. Technol. 37 (October (7)) (2013) 416–423.
[10] T.H.J. Yang, S.K.W. Leung, S. Phipps, R.L. Reuben, S.A. McNeill, F.K. Habib, A. Schnieder, R. Stevens, In-vitro dynamic micro-probing and the mechanical properties of human prostate tissues, Technol. Health Care 14 (4–5) (2006) 281–296.
[11] M. Aketagawa, T. Yashiki, S. Kimura, T.Q. Banh, Free spectral range measurement of Fabry–Pérot cavity using frequency modulation, Int. J. Precis. Eng. Manuf. 11 (December (6)) (2010) 851–856.
[12] X. Liu, I.I. Iordachita, X. He, R.H. Taylor, J.U. Kang, Miniature fiber-optic force sensor based on low-coherence Fabry–Pérot interferometry for vitreoretinal microsurgery, Biomed. Opt. Express 3 (May (5)) (2012) 1062–1076.
[13] M.-D. Zhou, C. Yang, Z. Liu, J.P. Cysyk, S.-Y. Zheng, An implantable Fabry–Pérot pressure sensor fabricated on left ventricular assist device for heart failure, Biomed. Microdevices 14 (February (1)) (2012) 235–245.
[14] S. Takeuchi, H. Tohara, H. Kudo, K. Otsuka, H. Saito, H. Uematsu, K. Mitsubayashi, An optic pharyngeal manometric sensor for deglutition analysis, Biomed. Microdevices 9 (December (6)) (2007) 893–899.
[15] N. Basumallick, I. Chatterjee, P. Biswas, K. Dasgupta, S. Bandyopadhyay, Fiber Bragg grating accelerometer with enhanced sensitivity, Sens. Actuators Phys. 173 (January (1)) (2012) 108–115.
[16] J. Kalenik, R. Pająk, A cantilever optical-fiber accelerometer, Sens. Actuators Phys. 68 (June (1–3)) (1998) 350–355.
[17] Z. Xiao, O. Engström, N. Vidovic, Diaphragm deflection of silicon interferometer structures used as pressure sensors, Sens. Actuators Phys. 58 (February (2)) (1997) 99–107.
[18] X. Huang, D. Zhang, A high sensitivity and high linearity pressure sensor based on a peninsula-structured diaphragm for low-pressure ranges, Sens. Actuators Phys. September (216) (2014) 176–189.
[19] S. Watson, M.J. Gander, W.N. MacPherson, J.S. Barton, J.D.C. Jones, T. Klotzbuecher, T. Braune, J. Ott, F. Schmitz, Laser-machined fibers as Fabry–Pérot pressure sensors, Appl. Opt. 45 (August (22)) (2006) 5590–5596.
[20] Y. Zhu, A. Wang, Miniature fiber-optic pressure sensor, IEEE Photonics Technol. Lett. 17 (February (2)) (2005) 447–449.
[21] W.N. MacPherson, S.R. Kidd, J.S. Barton, J.D.C. Jones, Phase demodulation in optical fibre Fabry–Pérot sensors with inexact phase steps, Optoelectron. IEE Proc. 144 (June (3)) (1997) 130–133.
[22] J. Chen, D. Chen, J. Geng, J. Li, H. Cai, Z. Fang, Stabilization of optical Fabry–Pérot sensor by active feedback control of diode laser, Sens. Actuators Phys. 148 (December (2)) (2008) 376–380.
[23] B. Yu, A. Wang, Grating-assisted demodulation of interferometric optical sensors, Appl. Opt. 42 (December (34)) (2003) 6824–6829.
[24] S. Phipps, T.H. Yang, S. McNeill, F. Habib, R. Reuben, The relationship between prostatic tissue morphology and mechanical properties: in vitro studies, Eur. Urol. Suppl. 2 (6) (2003) 47.
[25] S. Phipps, T.H.J. Yang, F.K. Habib, R.L. Reuben, S.A. McNeill, Measurement of tissue mechanical characteristics to distinguish between benign and malignant prostatic disease, Urology 66 (August (2)) (2005) 447–450.

Biographies

Jun Li graduated from Shanghai Institute of Optics and Fine Mechanics, Chinese Academy of Sciences (CAS) in 2007 with a Master's degree in Optical Engineering. After that he joined the PetroChina Pipeline Research Centre. His research interests there focussed on optical fibre sensing and its application for long distance oil and pipeline leak and safety monitoring. In 2010, Jun joined the Applied Optics and Photonics Group, Heriot-Watt University, and was awarded his Ph.D. degree in 2014 following his work on optical fibre interrogation of microcantilever sensors for biomedical applications.

Steven Hammer gained a Bachelor of Engineering (Honours) degree in Mechanical Engineering in 2000 from the University of Edinburgh. Following a research post at the same institution in 3D ultrasound and patient-specific blood flow modelling, he was awarded a Ph.D. in Medical Physics in 2009. He subsequently worked in the laboratory automation and prosthetics industries, and returned to academic research in 2012, joining the Institute of Mechanical, Process and Energy Engineering at Heriot-Watt University. He currently investigates methods of measuring soft tissue quality using *in vivo* mechanical measurements, and magnetic resonance elastography.

Wenmiao Shu received his B.Eng. degree in Polymer Materials from the Dalian University of Technology, China, in 1998, and a Ph.D. degree from the University of Cambridge in 2006. He is currently Associate Professor, Reader of Microengineering in the School of Engineering and Physical Sciences at Heriot-Watt University. His research interests cover a range of biomedical microengineering topics including micro-mechanical sensors and actuators, biosensors, lab-on-a-chip systems and 3D biofabrication.

Robert Maier graduated Dipl.Ing.FH in 1980 and received a Ph.D. in Physics in 2006. He worked as a researcher in various research institutions and in industry. In 1998 he joined Heriot-Watt University and is now in the Institute of Photonics and Quantum Sciences where he is leading a research group with a focus on fibre optic sensor technology. His latest research aims at the development of fibre sensors for use at very high temperatures for condition monitoring of metallic systems using Laser-based Additive Layer Manufacturing technology. Robert is an Honorary Fellow of Munich University of Applied Sciences.

Duncan Hand was awarded a Ph.D. by the University of Southampton in 1991 in optical fibre technologies. Later that year he moved to Heriot-Watt University, initially as a Research Associate working on optical sensing for manufacturing processes. In 1997 he was appointed Lecturer and subsequently Reader (2001) and Professor of Applied Photonics (2003). His current research activity focuses on laser-based manufacturing (micro-machining, micro-joining), optical fibre technology (delivery of high peak power laser light for manufacturing and surgery), and sensing (fibre optic sensors). He is currently Director of the EPSRC Centre for Innovative Manufacturing in Laser-based Production Processes.

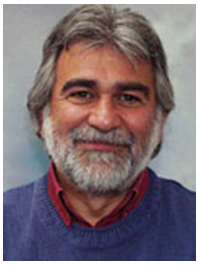

Robert L. Reuben is a Professor of Materials Engineering in the School of Engineering and Physical Sciences at Heriot-Watt University. He graduated with a First Class Honours in Metallurgy from the University of Strathclyde in 1974, after which he worked with the United Kingdom Atomic Energy Authority. In 1977 he joined the Open University's Oxford Research Unit researching the permeation characteristics to hydrogen and its isotopes of candidate fusion reactor containment materials, gaining a Ph.D. in that area in 1980. His research field includes experimental mechanics and microsystems engineering (often for medical applications), and sensor-based monitoring of machinery.

William N. MacPherson is an Associate Professor in Physics and a member of the Applied Optics and Photonics research group in the School of Engineering and Physical Sciences. His research interests are centred on the application of optical and fibre-optic techniques for measurement and instrumentation. This work includes high bandwidth temperature and pressure sensors for aerodynamic and explosion monitoring, novel fibres for structural monitoring, vibration and acceleration measurement, and studies into potential sensing applications of novel microstructured fibres. He has published over 90 journal and conference papers in this area.